Finite Element Analysis of hot Single Point Incremental forming of hip prostheses

Manel Sbayti[1,a], Andrea Ghiotti[2], Riadh Bahloul[1], Hedi Belhadjsalah[1] and Stefania Bruschi[2]

[1]*University of Monastir, National Engineering School, Mechanical Engineering Laboratory, Avenue Ibn El Jazzar, 5000, Monastir, Tunisia*
[2]*University of Padua, Department of Industrial Engineering, via Venezia 1, 35131, Padova, Italy*

Abstract. The titanium alloy Ti-6Al-4V is one of the most frequently used materials for biomedical applications due to its biocompatibility and excellent mechanical properties. However, wide usage of Ti-6Al-4V sheet is limited by its poor room-temperature formability. Therefore, hot Single Point Incremental Forming (SPIF) has been used to improve its formability. This paper aims at proving the feasibility of the hot incremental forming of an acetabular component of hip prosthesis by Finite Element simulations. The effect of process parameters, namely the forming temperature and the punch diameter on the geometric accuracy and the failure of the final product are investigated.

Keywords: Single Point Incremental Forming / High Temperature/ Formability / Ti-6Al-4V

1 Introduction

Single Point Incremental Forming (SPIF) is a variant of incremental forming suitable for prototyping and small batch production due to its flexibility and low tool effort. The flat sheets metals are progressively deformed using a hemispherical end forming tool whose path is generated in a CNC machining center or robot [1].

The selection of suitable technique for manufacturing of a specific product represents a complex issue. It is a multicriteria decision that depends on several factors regarding part design and complexity, material processing ability, desired accuracy, physical and mechanical properties of part, production quantity and cost, etc.

The technology of Incremental Sheet Forming (ISF) was primarily applied in the automobile and aerospace's industry [2, 3]. However, there are other branches with an important potential for the technology, such as the biomedical field. When addressing its use in medicine, it is possible to produce thin walled custom-made metal components. Araújo et al. [4] evaluated the SPIF process for producing titanium customized maxillofacial implants and demonstrated the role of this technology in manufacturing customized medical parts. Castelan et al. [5] presented the manufacturing by ISF of the custom-made cranial implants from a sheet of pure grade 2 titanium from Digital Image and Communications in Medicine (DICOM) images using 3D printing, CAD/CAM technology and incremental sheet forming. From Computerized Tomography (CT) images of a fractured skull, a CAD model of the skull BioModeling and a restorative implant were constructed digitally. Duflou et al. [6] used three different materials: AA1050, AISI 304 and medical grade titanium for accurate manufacture of cranio-facial implant using single point incremental forming process.

Fiorentino et al. [7] manufactured a plate prosthesis using a titanium alloy and Polycaprolactone (PCL). Although their results were promising, an optimization of the process parameters should be done in order to increase the accuracy of the part. The work of Milutinović et al. [8] has been focused on the manufacturing of a denture base (framework) of a complete denture by SPIF technology. The research included two different materials: carbon and stainless steel. They concluded that the new procedure enabled an additional mass reduction of the dental base (the final sheet thickness is 0.5mm instead 0.8mm of the original thickness) which is highly desirable from viewpoint of patient and comfort of wear.

Among biocompatible metallic materials, titanium and its alloys such as Ti-6Al-4V are increasingly used in biomedical applications due to their excellent properties such as corrosion resistance, strength-to-weight ratio and high toughness. However, Ti-6Al-4V possess low formability at room temperature. In order to improve the forming behavior of Ti6Al4V sheets, deformation under elevated temperatures is needed. Therefore, multiple concepts for warm ISF processes were recently developed and introduced in the technical literature [9, 10]. It was shown that, by using hot ISF process, the formability of lightweight alloys among them Ti-6Al-4V can be significantly improved [11, 12, 13, 14].

[a] Manel Sbayti: manelasbayti@gmail.com

The present paper aims to provide a preliminary numerical study of hot single point incremental forming technology using the commercial finite element computer program ABAQUS. The main objective of these research works is to evaluate the feasibility of producing customized acetabular component of hip prosthesis with an acceptable geometrical accuracy with this process and based on the use of biocompatible materials such as Ti-6Al-4V titanium alloy.

Figure 1 represents the component of hip prosthesis to be studied in the present work.

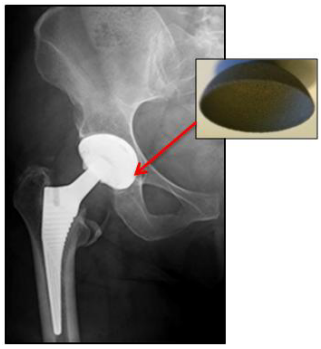

Figure 1. The studied part of hip prosthesis.

2 Finite element aspects and material modeling

The accuracy of Finite Element Method (FEM) in the simulation of metal forming processes depends both on the constitutive laws used and their material parameters identification. In order to simulate the SPIF process, temperature dependence is taken into consideration in the current simulation.

2.1 Material

2.1.1 Punch material

The material used for the hemispherical tool was the SM30 tungsten carbide. Table 1 shows the thermos-physical properties of the punch material.

Table 1. Thermo-physical material parameters [15].

Material parameters of the tool	**Values**	
Density ρ [Kg/m³]	12800	
Poisson's ratio υ	0.22	
Young's modulus E [MPa]	630000	
Heat conductivity λ [W/(m·°C)]	T (°C)	Value
	23	44.6
	600	59
	800	51.2
Specific heat C_p [J/(kg·°C)]	T (°C)	Value
	20	226
	320	296
	520	326
	820	342

2.1.2 Sheet material

The sheet material used in the numerical simulation is the Ti6Al4V alloy. The mechanical and thermo-physical properties of the Ti-6Al-4V alloy are defined as temperature (T) dependent. The thermo-physical material parameters used for the work piece are compiled in Table 2.

Table 2. Thermo-physical material parameters [16].

Material parameters of Ti-6Al-4V sheet	**Values**
Density ρ [Kg/m³]	4430
Poisson's ratio υ	0.22
Young's modulus E [MPa]	E(T)= 0.7412T+113375
Thermal expansion α [1/°K]	8.9E-6
Heat conductivity λ [W/(m·°C)]	λ(T)= 7.039 $e^{0.0011T}$
Specific heat C_p [N/(mm²·°C)]	C_p(T)= 2.24 $e^{0.0007T}$

2.1.3 Material constitutive model

The parameters for the Johnson-Cook (J-C) constitutive model of a biomedical grade Ti6Al4V alloy were determined for the numerical modelling of its deformation in the warm SPIF process. So, the J-C flow stress is proposed as the applied material model for the workpiece in this study. It considers simple forms of empirical relations of stress with strain, strain rate and temperature as follows:

$$\sigma_f = \left(A+B\cdot\bar{\varepsilon}_{pl}^{n}\right)\cdot\left[1+C\cdot\ln\left(\frac{\dot{\bar{\varepsilon}}}{\dot{\varepsilon}_0}\right)\right]\cdot\left[1-\left(\frac{T-T_{room}}{T_m-T_{room}}\right)^{m}\right] \quad (1)$$

where, A, B, n, C and m are the constants of material, $\dot{\bar{\varepsilon}}$ is the strain rate which is normalized with a reference strain rate $\dot{\varepsilon}_0$ ($1s^{-1}$). T_{room} represents the room temperature and T_m is the melting temperature of the material equal to 1604°C. The parameter n takes into account the strain hardening effect and the two coefficients m and C model respectively the thermal softening effect and the strain rate sensitivity. The identified Johnson-Cook constitutive model parameters relative to the used material are illustrated in Table 3.

Table 3. Constants of the Johnson-Cook constitutive model for the Ti-6Al-4V alloy.

A (MPa)	B (MPa)	C	n	m
460	1450	0.08	1.31	0.85

2.2 Description of the numerical model

As the SPIF process involves large material deformation without the presence of the dies, suitable algorithm should be employed in the FEA. In this investigation, a three-dimensional thermo-viscoplastic FE model is set up for the simulation of the SPIF process to obtain thermos-mechanical responses of the process. The numerical computations were performed with the commercial code ABAQUS/EXPLICIT software.

2.2.1 Tool trajectory

The tool path design is fundamental in the design of the SPIF processes, since it impacts on the dimensional accuracy, surface finish, formability, thickness variation and processing time. The punch movement must be gradual in order to progressively deform the sheet. The tool path is prescribed by the Numerical Control (NC) data that is generated from a CAD model of the component to be formed. The forming strategy consists of a single forming stage where the tool traces along a sequence of contour lines with a vertical increment step size (Δz = 0.2 mm) in between. In all the simulations, the diameter of the tool was 10 mm. The shape of the titanium alloy sheet Ti-6Al-4V has been considered square for different temperature values with a size of 90 mm× 90 mm × 1mm.

The part is formed according to the tool trajectory presented in Figure 2. The considered tool path is made up of a series of contours generated transverse to the long axis of the real part. The forming tool follows to the predetermined tool path and gradually forms the sheet metal in a series of incremental steps until the final depth is reached.

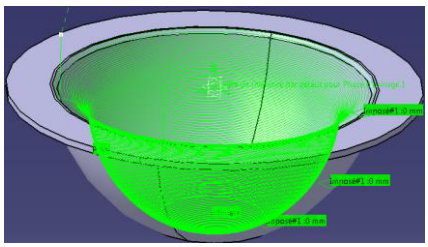

Figure 2. Schematic description of the tooling path generated by CATIA and integrated into ABAQUS.

2.2.2 Boundary conditions

Modeling the interaction between the tool and the sheet is one of the most important considerations necessary to simulate the incremental forming process correctly. The interaction properties between the sheet and the contact area with the punch are defined by the Coulomb's friction model expressed as follows :

$$\tau_{fric} = \mu P \tag{2}$$

where τ_{fric} is the friction shear stress, μ the friction coefficient and P the normal contact pressure. Hence, a fraction of dissipated energy converted into heat is tacked into account. the heat generation from the friction is described as follows: So, the rate of frictional energy dissipation is described as follows:

$$q_{fric} = \eta\dot{\gamma}\,\tau_{fric} = \eta\dot{\gamma}\mu P \tag{3}$$

where $\dot{\gamma}$ is the slipping rate and η the fraction of dissipation energy converted into heat.

The sheet blank is experimentally supported on a four-sided fixture and is clamped rigidly to this fixture with a backing plate to support the punch displacement. From numerical point of view, the sides of the initial blank are fixed in all directions and for each simulation, a uniform temperature has been applied to the entire sheet (Figure 3).

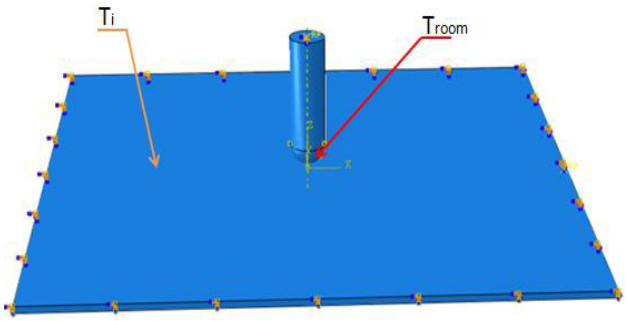

Figure 3. Three-dimensional exploded view of numerical model used in SPIF at high temperatures.

2.2.3 Finite element mesh

The finite element meshing subdivision of the initial sheet is depicted in Figure 4. In the FE model, eight-node thermally coupled brick, with trilinear displacement and temperature, reduced integration and hourglass control (C3D8RT) were applied in the fully coupled thermal analysis to model the sheet blank. In the numerical calculations, the sheet was meshed in three layers in the thickness direction to take into account of bending stiffness and the global size of elements is 0.8 mm×0.8 mm

Also, in this study, the forming tool has been meshed using 4-node thermally coupled tetrahedron elements (C3D4T), linear in displacement and temperature.

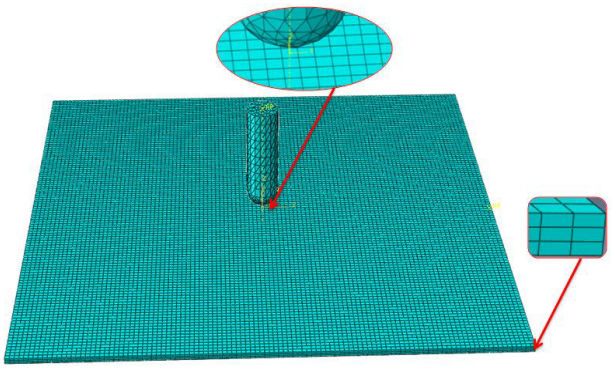

Figure 4. The finite element meshing configuration of the initial blank.

3 Results and discussions

3.1 Forming temperature influence

In Figure 5 are pictured the 3D iso-values of the final reached temperature distributions for various initial forming temperatures. Figures 6a$_1$, a$_2$, a$_3$ and a$_4$ report the simulated incremental forming sequences, and highlight the calculated temperature histories of the final part respectively for the forming temperatures T of 20°C, 400°C, 500°C and 600°C.

As it can be concluded from figures 6ai, the calculated final temperatures at the end of the process simulations increase due to initial sheet heating and to heat generation during the process. It can also be observed from these figures that the temperature distributions agree with the position of the tool on the sheet.

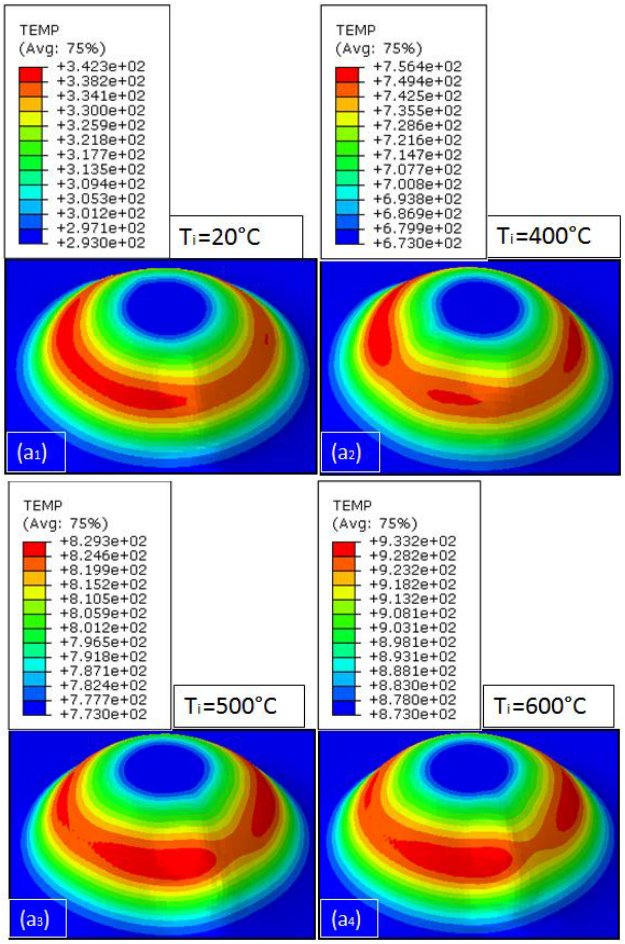

Figure 5. Temperature contours at the sheet surface calculated by FE modeling for various temperatures.

A coordinate system is assigned to the simulated model to measure set of points on profile of upper mesh layer (the model is meshed in three layers). Results are taken along a radial path after the removal of the backing plate, which is shown in Figure 6.

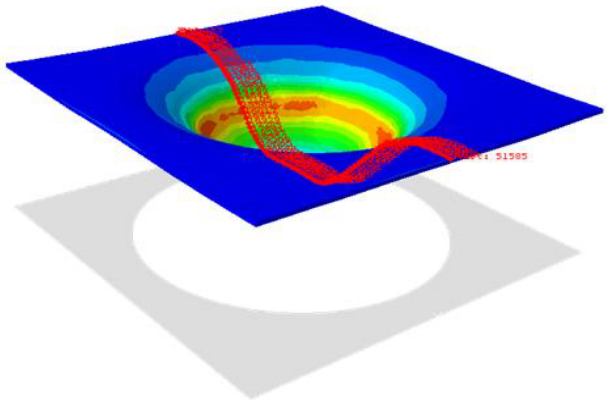

Figure 6. Final shape of parts with a global heating: radial path definition monitored during the simulation for measuring the depth profiles.

Figure 7 illustrates the thickness distribution versus radial distance (Figure 6) formed at various temperatures: Ti = 20°C, 400°C and 600°C. There is a rigorous reduction in thickness in the stressed areas and a fixing thickness to its initial value at the bottom of the sheet. At high temperature the distribution of the thickness is more homogeneous.

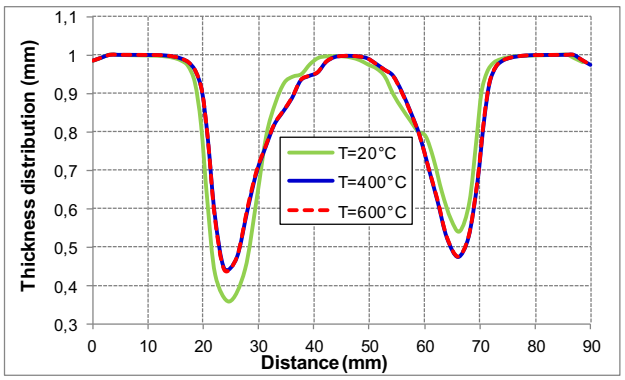

Figure 7. Thickness distribution versus radial distance formed at various temperatures: Ti = 20°C, 400°C and 600°C.

Figure 8 represents the final profiles of the part according to the radial distance from the clamped corner described in Figure 6. Compared to the conventional process, this strategy can dramatically improve geometric accuracy, since the springback effects decrease as the temperature increases.

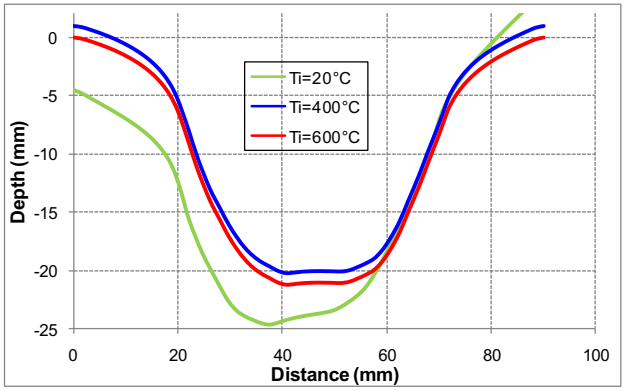

Figure 8. Depth profiles of hip prosthesis versus radial distance formed at various temperatures: T_i = 20°C, 400°C and 600°C.

3.2 Punch diameter influence

Figure 9 shows the evolution of the temperature along a radial path at T = 400°C with the variation in punch diameter of 6, 8 and 10 mm values. Thus, the dependence of the punch position on distribution of the final state of a temperature against the sheet and after the accumulation of numerous incremental deformation passes throughout the process proves to be logical. It can be noted that the smaller the tool size the higher the temperature calculated by the FE model.

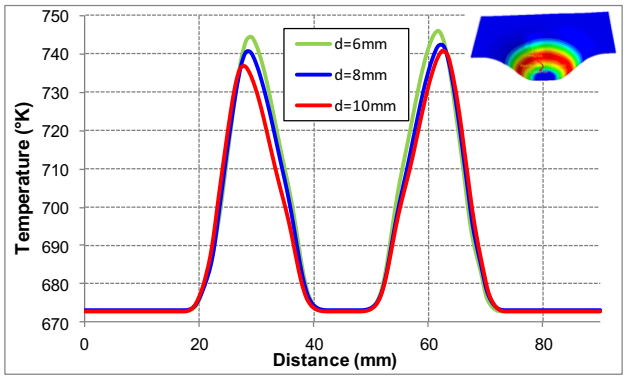

Figure 9. Temperature distributions along the radial path predicted by FEM for different punch diameter variations : a_1) d = 6mm, a_2) d = 8mm, a_3) d = 10mm at T = 400°C.

3.3. Thermo-viscoplastic material behaviour coupled with damage

Damage model proposed by Johnson-Cook is used in conjunction with J-C yield model. According to classical damage law, the theoretical expression of this response in a finite element representative of fracture or macro-crack initiation resulting from the material damage of workpiece is defined by:

$$D = \sum \frac{\Delta \bar{\varepsilon}}{\bar{\varepsilon}_f} \tag{4}$$

where $\Delta\bar{\varepsilon}$ is the increment of equivalent plastic strain during an integration step, and $\bar{\varepsilon}_f$ is the equivalent strain value at fracture under current conditions. The initiation of cracking and damage of product is then allowed to occur when this damage variable reached its critical value (D = 1) in any element and the concerned one is removed from computation. According to Johnson-Cook damage law, the general formulation of the fracture strain at critical damage can be written as:

$$\bar{\varepsilon}_f = \left[D_1 + D_2.\exp\left(D_3\eta\right)\right] \times \left[1 + D_4.\ln\left(\frac{\dot{\bar{\varepsilon}}}{\dot{\bar{\varepsilon}}_0}\right)\right] \times \left[1 + D_5.\left(\frac{T - T_{room}}{T_m - T_{room}}\right)\right] \tag{5}$$

where the Johnson-Cook damage parameters are represented in the following forms:

D_1: Initial failure strain,
D_2: Exponential factor,
D_3: Triaxiality factor,
D_4: Strain rate factor,
D_5: Temperature factor,

η: The ratio of the hydrostatic pressure to the effective stress

The Titanium 6Al-4V failure strain parameters are summarized in Table 4.

Table 4. Johnson-Cook failure parameters for Ti-6Al-4V.

D_1	D_2	D_3	D_4	D_5
-0.09	0.25	-0.5	0.014	3.87

3.3.1 Influence of heating temperature on damage field distribution

Figure 10 shows the iso-values of the scalar damage parameter modeled by the Stiffness Degradation SDEG during the forming process at four different temperatures. It should be noted that SDEG = 1.0 means that the corresponding elements failed and a crack occurred. According to these results, the critical damage appears at room temperature since the SDEG value is very close to 1 in the contact region between punch and sheet. As expected in these conditions, the damage variable increased which confirm the previous result that the forming of the part doesn't occur at Ti = 20°C.

These results are presented at the same time when the maximum degradation appeared in the part at room temperature. Hence, the damage variable SDEG is investigated at the same frame for the different temperature values (approximately the middle of the step). As expected, at T_i = 20°C the part is completely damaged in a while frame, because as we have cited that the Ti-6Al-4V titanium alloy has a very poor formability at room temperature. However, at T ≥ 400°C and at the same time of the step calculation, the part is not damaged since the damage parameter SDEG is much lower to 1. This conclusion is proved by the experiences of several authors among them we can cite G. Fan et al. [11].

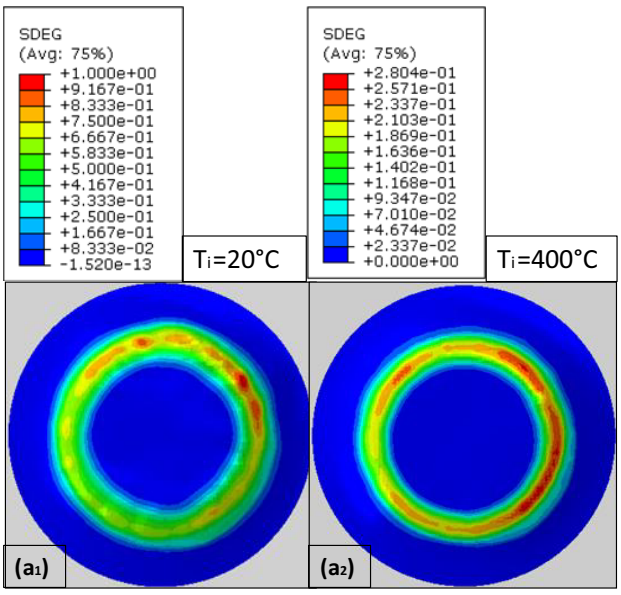

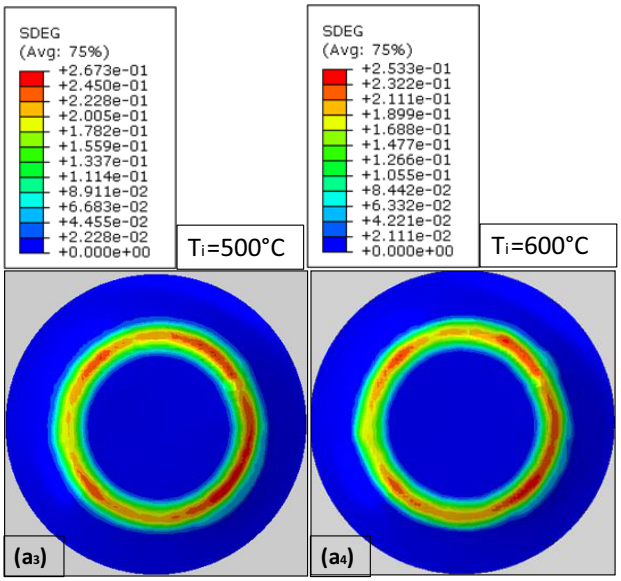

Figure 10. 3D iso-values of the Stiffness Degradation SDEG obtained by FEM calculation for various temperatures: a_1) T_i = 20°C, a_2) T_i= 400°C, a_3) T_i = 500°C, a_4) T_i = 600°C at the middle of the step.

According to the same path previously indicated in Figure 6, the final geometry was predicted at three temperatures after removal of the backing plate, as shown in Figure 11. Such a thermos-mechanical problem results in appearance of springback effect after the stress relaxation during the forming of thin Ti-6Al-4V sheets. Figure 11 reports the numerical results in terms of the final depth reached along the meridian direction in parametric form.

So, taking into account the damage effect, it was observed that the maximum final depth cannot exceed 8.77 mm at room temperature (Ti =20°C). The plasticity of the Ti-6Al-4V alloy at 500°C is better than that at room temperature, therefore the ductility is greatly enhanced, and the yield stress is reduced in half [17]. In the investigated range, a temperature from 400 to 600°C should be selected to achieve a better formability in terms of forming penetration and geometrical accuracy.

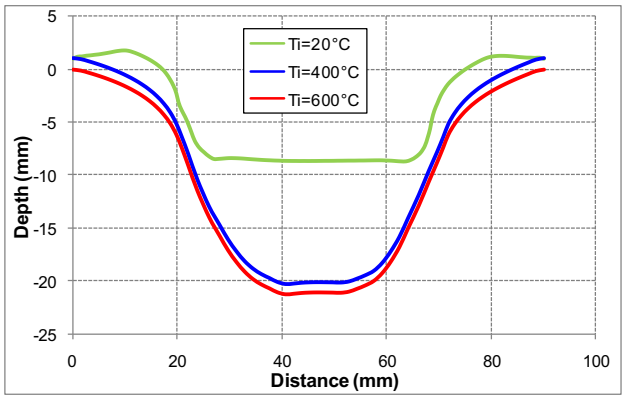

Figure 11. Evolution of depth profiles versus radial distance.

3.3.2 Influence of punch diameter on damage field distribution at T = 400°C

Figures 12a1, a2 et a3 show the evolution of the accumulated damage defined by stiffness degradation SDEG for various tool diameters. As illustrated in Figure 12, there are no damaged elements at T = 400°C with the three tool diameters (6, 8 and 10 mm). At the end of sheet forming operation, the SDEG values are close and doesn't exceed 0.547, proving that the parameter punch size has a small effect on the damage generation. Finally, it can be concluded that the effect of forming temperature is more important on the geometric accuracy of the part.

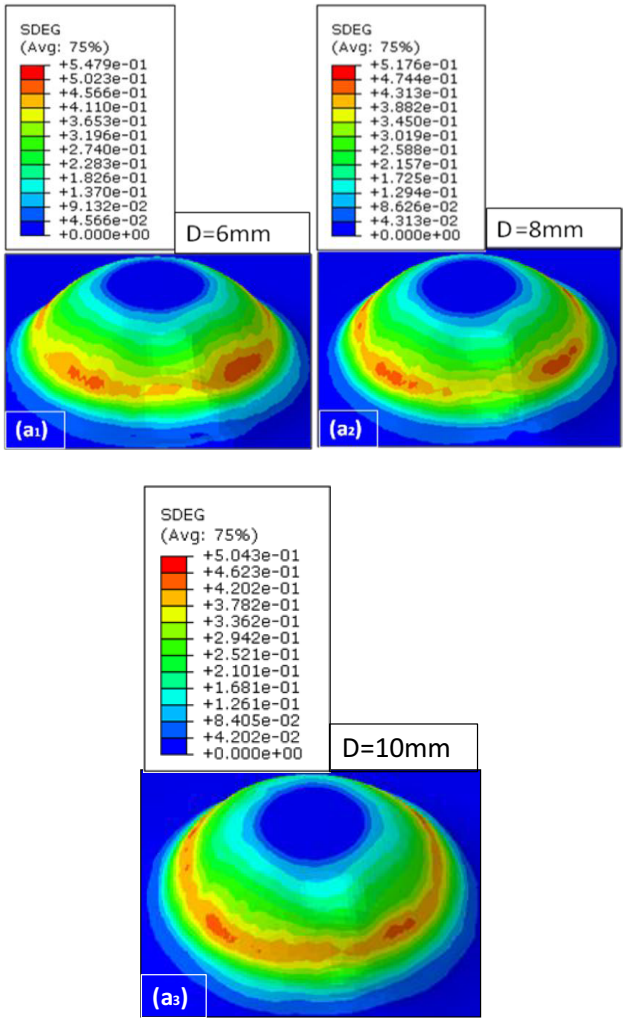

Figure 12. 3D iso-values of the Stiffness degradation SDEG obtained by FEM calculation for various punch diameters: a_1) d = 6 mm, a_2) d = 8 mm, a_3) d =10 mm at the middle of the step.

4 Conclusions

In this work, by evaluating FE simulation of hot SPIF process for an acetabular component, the feasibility of manufacturing customized titanium hip by using the ISF approach is studied and the particular issues and possible solutions were discussed. The conclusions of this work may be summarized as follows:

1) ISF of acetabular by using Grade 5 titanium sheets is a feasible solution and it shows clearly the potential for real medical application.
2) The geometry accuracy is improved at T ≥ 400°C
3) First results show promise and the process seems to be satisfactory for the application of hip prosthesis.
4) Further development is still needed to evaluate the effect of the majority of process parameters on the formability of the part to optimize these parameters for the experimental study.

In the paper presented, possibilities of applying SPIF technology to produce a metal acetabular of hip prosthesis have been numerically investigated.

References

1. M. Callegari, D. Amodio, E. Ceretti, C. Giardini, In: Low, K. (Ed.). Pro Literatur Verlag, Germany, pp. 493–514 (2006)
2. W.B. Lievers, A.K. Pilkey, D.J. Lloyd, Acta Mater **52**(10):3001–3007 (2004)
3. G. Hussain , H. R. Khan , L. Gao, N. Hayat. Mater Manuf Process **28**(3):324–329 (2012)
4. R. Araújo, P. Teixeira, M.B. Silva, A. Reis, , P.A.F. Martins, Key Eng. Mat., 544–557: 1388–1393 (2013).
5. J. Castelan, L. Schaeffer, A. Daleffe, D. Fritzen, V. Salvaro, FP. Silva. Revista Brasileira de Engenharia Biomédica. **30**(3):265-73 (2014)
6. Duflou JR, Behera AK, Vanhove H, Bertol LS. Key Engineering Materials. 549:223-30 (2013)
7. A. Fiorentino, G.P. Marenda, R. Marzi, E. Ceretti. In: Proceedings of the 5th International Conference on Advanced Research in Virtual and Rapid Prototyping. p. 589-594 (2011)
8. M. Milutinović , R. Lenđel, M. Potranb , D. Vilotić, P. Skakuna, M. Plančak. Journal for Technology of Plasticity, Vol. **39** Number 2, (2014)
9. G. Fan, L. Gao, G. Hussain, Zhaoli Wu. International Journal of Machine Tools & Manufacture **48** 1688–1692 (2008)
10. A. Göttmann, J. Diettrich, G. Bergweiler, M. Bambach, G. Hirt, P. Loosen, R. Poprawe. Production Engineering - Research and Development, **5** (3), 263-271.(2011)
11. G. Fan, F. Sun, X. Meng, L. Gao, G. Tong. Int J Adv Manuf Technol **49**:941–947 (2010)
12. P. Homola, L. Novakova, V. Kafka, Mariluz P. Oscoz, Int J of Chemical, Molecular, Nuclear, Materials and Metallurgical Engineering Vol:**8**, No:1, 2014
13. M. Honarpisheh, M. J. Abdolhoseini, S. Amini. Int J Adv Manuf Technol (2015)
14. R. Liu, B. Lu, D. Xu, J. Chen, F. Chen, H. Ou, H.Long. Int J Adv Manuf Technol (2015)
15. F. Zemzemi. PhD thesis: Central School of Lyon, pp. 92-93, (2007)
16. T. Ozel, M. Sima, A. Srivastava, Finite Element Simulation of High Speed Machining Ti-6Al-4V Alloy using Modified Material Models, Transactions of the NAMRI/SME, Vol.**38**, pp. 49-56, (2010)
17. R.S. Lee, H.C. Lin. Journal of Materials Processing Technology **79** 224–235 (1998)